Probing the magnetic structure of $EuPtIn_4$ via x-ray resonant magnetic scattering

J. R. L. Mardegan, S. Francoual, L. S. I. Veiga, J. Vogel, and J. Strempfer
Deutsches Elektronen-Synchrotron (DESY), Hamburg 22607, Germany

M. Saleta, P. Pagliuso, P. Rosa, and E. Granado
Instituto de Física "Gleb Wataghin," Universidade Estadual de Campinas, Campinas, São Paulo 13083-859 Brazil

(Dated: July 21, 2017)

X-ray resonant magnetic scattering technique reveals that the magnetically ground state for the $EuPtIn_4$ compound is an incommensurate antiferromagnetic spin structure with a propagation vector type $(\frac{1}{2}, \frac{1}{2}, \tau)$. The scattering measurement conducted without an external magnetic field corroborates the macroscopic finds in which the system shows a second order phase transition from a paramagnetic to an antiferromagnetic state below $T_N = 13.13(4)$. Despite the low temperature phase transition, the resonance magnetic scattering displays a strong enhancement of the magnetic signal around the Eu L_2 edge in which indicates a strong magnetic interaction through a highly spin-polarized surrounding. In addition, the temperature dependence reveals that the τ component of the propagation vector locks at ~ 0.428 and there is no indication of additional magnetic transition induced by temperature. Resonant scattering measurements conducted at low temperature and in absence of magnetic field exhibit a magnetic structure in which the Eu spins are aligned parallel to the (1,-$\frac{1}{2}$,-1). However, we note that the magnetic moments rotate to the $(0, 1, 1)$ direction when an external magnetic field higher than 3.5 T is applied along the a-axis. The observation of the incommensurate magnetic phase and a spin-flop transition in this new class of materials bring new opportunities to investigate new quantum fluctuation systems based on Eu ions.

I. INTRODUCTION

The search for fascinating materials with interesting electronic and magnetic properties has led to an enormous development in diverse areas of condensed matters physics. In particular, the Indium-rich materials containing rare earth and transition metal elements have been widely studied due to the ability to form In clusters and to host exotic physical phenomena raised from the competition or even the cooperation among the Ruderman-Kittel-Kasuya-Yosida (RKKY) magnetic interaction, heavy fermion (HF) behavior, crystalline electric field (CEF) and Kondo effects.[1–3] Examples of such materials with these properties are the so-called 115 ($RT\text{In}_5$, R - rare earth, T = Co, Rh, Ir) in which the $4f$ orbitals and the conduction electrons play a valuable role in the electronic, magnetic and structural properties.[3–5]

Following similar receipts to obtain complex and exotic systems based on In and 3-5d elements, a new class of materials composed by $RX\text{In}_4$ (with R = rare earth, and T = transition metal) was synthesized. These new materials with $YNiAl_4$ structure[6] exhibit an intricate framework of bonds in which are formed three-dimensional $X\text{In}_4$ networks with the In and the transition metal ions placed very close to each other (In-In: $\sim$3 Å; In-T: $\sim$2.5 Å). The symmetry of these compounds are ruled by the space group $Cmcm$ (No. 163) in which the In ions occupy three different inequivalent sites ($4a$, $4c$, and $8f$), whilst the transition metals T and the R ions are located at the Wyckoff position $4c$.[7–10] This complex network of ions strongly affects the electronic and magnetic properties as it will discuss below. Besides the puzzling structure, these materials have drawn attention due to the fact that the crystals can be only synthesized with alkaline earth or few rare earth elements at the crystallographic position $4c$. The possible elements from the lanthanide series are Ce, Yb, and Eu in which the firsts two are routinely found on HF materials and the third exhibits a quenching of the orbital. Since these rare earth elements are present, the materials have exhibited a series of magnetic transitions as a function of temperature and magnetic field.[9–15] For instance, $CeNiIn_4$ and $EuPdIn_4$ materials exhibit at low temperatures two lambda-type anomalies in the specific heat data due to magnetic ordering and spin reorientations induced by magnetic field applied along different crystallographic directions.[11,13–15]. Although the crystallographic and the macroscopic magnetic properties of these class of materials have been widely investigated in the last decade, the magnetic structure is still unknown.

To better understand the microscopic magnetic properties of this family, we have chosen the $EuPtIn_4$ compound as our candidate. Europium based materials with 2+ valence have only a Spin-state ($L = 0$ and $S = 7/2$) and therefore the magnetic properties are mainly established by the RKKY interactions. Other magnetic interactions or CEF effects can be neglected and therefore they do not influence the magnetic structure. In addition, large and high quality single crystal of $EuPtIn_4$ can be synthesized and are ideal to probe with x-ray instead of neutron magnetic scattering techniques. Transport and magnetic properties have been recently published for this material by at least two independent research groups in which there are few issues mainly concerning the magnetic properties.[9,12–15] The general consensus is related to an antiferromagnetic ordering around 13 K in which the long b-axis is the hard axis. However, there are two anomalies observed as a function of temperature (T^* at approximately 12.8 K and 5.5 K) and an anomaly ob-

served in the isothermal magnetization curves. The features at T^* were initially addressed as possible a spin-reorientation or second AFM ordering and the kink in the magnetization curve as a possible spin-flop transition. In this sense the x-ray resonance magnetic scattering (XRMS) technique becomes a powerful tool to solve these issues and also to determine the magnetic structure.

Here we determine the magnetic structure at low temperature of $EuPtIn_4$ compound with and without an external magnetic field using XRMS technique. The XRMS measurements reveal an incommensurate (ICM) antiferromagnetic phase below Néel temperature (T_N = 13.13(4) K) with a magnetic propagation vector $(\frac{1}{2}, \frac{1}{2}, \tau)$ with $\tau \sim 0.43$. The magnetic peaks measured with the x-ray energy tuned to the Eu L_2 edge show an enhancement of around two orders of magnitude which suggests a strong spin polarization of the $5d$ bands by the $4f^7$ states. At low temperature and zero magnetic field, the resonant measurements indicate that the Eu magnetic moments are following the (1,-1/2,-1) direction. In addition, a spin-reorientation which corroborates the finding observed in Ref. 15 is observed when $H > 3.5$ T is applied parallel to the crystallographic direction a. A second anomaly reported at 12.8 K in macroscopic measurements was not observed in our temperature dependence measurements which might indicate a non-magnetic character. Our resonant magnetic studies open new opportunities to explore this class of materials with several magnetic transitions and incommensurate structure.

II. EXPERIMENTAL DETAILS

A high quality single crystal of $EuPtIn_4$ with approximate size 1 x 1 x 0.4 mm^3 was grown at University of California Irvine by an In self flux method similar as reported previously elsewhere.[12] Néel temperature, effective magnetic moment and Curie-Weiss constant were verified by macroscopic measurements.[9,12,15]

X-ray resonant magnetic scattering measurements were carried out at beamline P09 at PETRA III (DESY, Hamburg/Germany).[16] The measurements performed in the absence of magnetic field were conducted with the sample mounted inside a closed-cycle displex cryostat with the b-axis specular and the a-axis pointing parallel to the incoming beam. For the measurements conducted under magnetic field (up to 8 T), the single crystal was mounted inside the superconductor magnet in a horizontal scattering geometry in which the magnetic field was applied almost parallel to the a-axis with a tilt angle of approximately 10°.

Magnetic superlattice reflections type $(\pm\frac{1}{2}, \frac{K}{2}, \tau)$ with $K = (2n+1)$ were measured below and across the magnetic phase transition temperature. To determine the Eu magnetic structure, full polarization analysis (FPA)[17–20] was performed in selected magnetic reflections. To enhance the magnetic signal, the measurements were performed with the energy beam tuned to the Eu L_2 absorption edge (7617 eV) where we are probing the transition from the initial $2p_{1/2}$ to the intermediate $5d$ states.

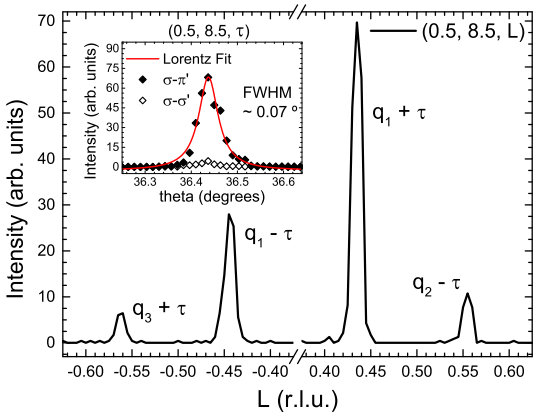

FIG. 1. (Color online) Reciprocal space L-scan performed across the $(\frac{1}{2}, \frac{17}{2}, 0)$ reflection at low temperature (7.5 K). The inset displays the $(\frac{1}{2}, \frac{17}{2}, \tau)$ reflection for both $\sigma - \sigma'$ and $\sigma - \pi'$ polarization channels. The solid red line is a fit to a Lorentzian function peak shape.

III. EXPERIMENTAL RESULTS

A. Magnetic structure in zero magnetic field

Figure 1 shows an L-scan through the $(\frac{1}{2}, \frac{17}{2}, L)$ magnetic reflection at 7.5 K. The satellites peaks shown in Fig. 1 demonstrate that the magnetic structure can be related to an incommensurate phase with a propagation vector type $(\frac{1}{2}, \frac{1}{2}, \tau)$ with $\tau = 0.4258$. In addition, the inset in Fig. 1 reports that the magnetic contribution is only observed in the π'channel, which is characteristic of dipole-dipole electric transition in the case of σ incident polarization. The observed propagation suggests a doubling of the chemical unit cell in the a- and b-crystallographic directions while along the c-direction the magnetic unit cell is composed by approximately 7 chemical unit cells.

To probe the magnetic character of those reflections, energy and temperature dependence were carried out below and across T_N. On Figure 2 the energy of the incoming beam is scanned near the magnetic reflection $(\frac{1}{2}, \frac{17}{2}, \tau)$ at two different polarization channels ($\sigma - \pi'$: panel 2(a); and $\pi - \pi'$: panel2(b)). The two polarization channels with similar intensities may suggest that this composed has a complex magnetic spin structure. The Fig. 2 also shows that the maximum resonant peak intensity is found $\sim$ 2-3 eV above the absorption edge (7617 eV for the Eu L_2 edge)[21] as a consequence of dipole electronic transition[22]. In addition, the inset in panel 2(a) shows the normalized absorption coefficients (μ) obtained from the fluorescence yield in which only contributions from the magnetic Eu^{2+} ions ($4f^7$, $J = 7/2$, magnetic) are observed. The resonant enhancement of the intensity

(over two orders of magnitude) observed in the insets at the magnetic peak position confirms the overlap between the $2p/5d$ orbitals and a strong exchange interaction between the localized electrons at the $4f$ shells and the extend $5d$ bands.

The evolution of the integrated intensity at the magnetic Bragg reflections as a function of temperature for the $\pi - \pi'$ polarization channel is displayed in Figure 3. Intensity, width and peak position are obtained fitting the L-scan through the magnetic peak $(\frac{1}{2}, \frac{23}{2}, \tau)$. The temperature evolution data is fitted by a power-law expression type $(1 - T/T_N)^{2\beta}$ close to the phase transition in which yields $T_N = 13.13(4)$ K and critical exponent $\beta = 0.42(3)$. The value of T_N agrees with bulk macroscopic measurements[9,12], while the β exponent is higher than expected for a three-dimensional (3D) Heisenberg magnetic model.[23,24] Besides these parameters, the peak width and the τ position (center position) were recovered from the temperature dependence fitting. As shown as insert in Fig. 3(b) and 3(c), there are no apparent broadening of the magnetic peak and variation in the τ component of the propagation vector up to the Néel temperature. The correlation length (ξ) along the c-axis obtained from the temperature dependence is $\xi \sim 3700$ Å (or ~ 500 unit cells).

Since this material has an unknown magnetic structure, we combine XRMS measurements and symmetry analysis to determine the magnetic moment direction and therefore solve the magnetic structure. The knowledge of the propagation vector and the crystal structure is required to obtain the irreducible representation (IR) through for instance the SARAh program.[25] Considering

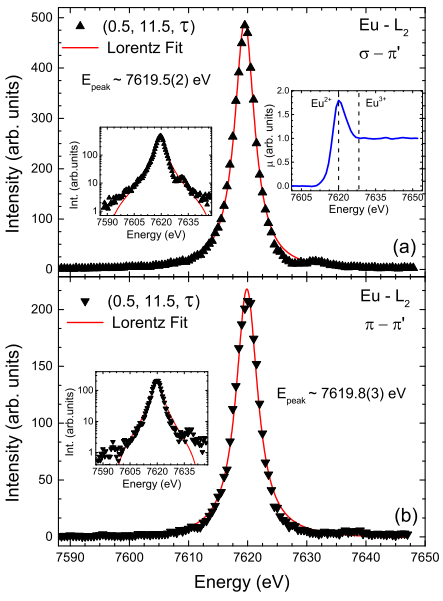

FIG. 2. (Color online) Energy dependence obtained through the Eu L_2 absorption edge at 7.5 K for the $(\frac{1}{2}, \frac{23}{2}, \tau)$ magnetic reflection at the (a) $\sigma - \pi'$ and (b) $\pi - \pi'$ polarization channels. The intensities are obtained with one second integration time.

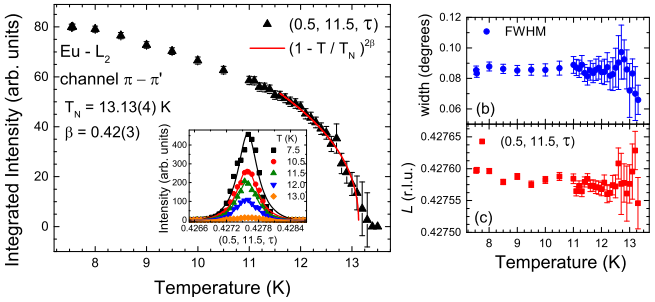

FIG. 3. (Color online) Temperature evolution of the $(\frac{1}{2}, \frac{23}{2}, \tau)$ magnetic reflection in the $\pi - \pi'$ polarization channel. Panel (a) exhibits the temperature dependence of the integrated intensity obtained with L-scan along the $(0, 0, L)$ direction in zero magnetic field. The inset shows L-scan around the magnetic peaks for different temperatures, the T_N and the critical exponent β obtained from a critical power-law fitting $(1 - T/T_N)^{2\beta}$ (solid red curve). Panels (b) and (c) exhibit the evolution of the peak width and L component through the temperature transition.

that the $EuPtIn_4$ compound exhibits a magnetic propagation vector $(\frac{1}{2}, \frac{1}{2}, \tau)$ (point D in the Brillouin zone, and with the star of the k-vector with 4 arms), and the magnetic Eu^{2+} ions occupy the $4c$ Wyckoff position, the SARAh returns the possible IR's for this material. The obtained magnetic representation (MR) is decomposed into two non-zero IR's (Γ_1 and Γ_2), and they are summarized in Table I with their respective basis vectors (ψ). As we can see in Table I, the main difference between the Γ_1 and the Γ_2 representations is related to the coupling between the Eu ions. Both irreducible representations allow the magnetic moments to point in any direction, since there is no constrain in the moment direction.

TABLE I. Basis vectors (BV's) for the space group $Cmcm$ with $\mathbf{k} = (\frac{1}{2}, \frac{1}{2}, \tau)$. The decomposition of the magnetic representation (MR) for the Eu site can be written as: $\Gamma_{Mag} = 3\Gamma_1^1 + 3\Gamma_2^1$. The two rare earth atoms positions of the non-primitive basis are defined according to 1: $(0, 0.374, 0.25)$ and 2: $(0, 0.626, 0.75)$.

			BV components					
IR	BV	Atom	$m_{\parallel a}$	$m_{\parallel b}$	$m_{\parallel c}$	$im_{\parallel a}$	$im_{\parallel b}$	$im_{\parallel c}$
Γ_1	ψ_1	1	1	0	0	0	0	0
		2	0.22	0	0	0.98	0	0
	ψ_2	1	0	1	0	0	0	0
		2	0	0.22	0	0	0.98	0
	ψ_3	1	0	0	1	0	0	0
		2	0	0	-0.22	0	0	-0.98
Γ_2	ψ_4	1	1	0	0	0	0	0
		2	-0.22	0	0	-0.98	0	0
	ψ_5	1	0	1	0	0	0	0
		2	0	-0.22	0	0	-0.98	0
	ψ_6	1	0	0	1	0	0	0
		2	0	0	0.22	0	0	0.98

To distinguish the magnetic structures, we measured several magnetic reflections along the $(\frac{1}{2}, \frac{K}{2}, \tau)$ direction in the $\sigma - \pi$' polarization channel. The integrated intensity obtained for each reflections assuming only dipole transition is:[26–28]

$$I_{\sigma\pi'} = A \left| \sum_n f_n^{E1} e^{i\vec{q}\cdot\vec{r}_n} \right|^2, \\ = A \left| f_1^{E1} e^{2\pi i(\frac{1}{2},\frac{k}{2},\tau)\cdot\vec{r}_1} + f_2^{E1} e^{2\pi i(\frac{1}{2},\frac{k}{2},\tau)\cdot\vec{r}_2} \right|^2, \quad (1)$$

where

$$A = \frac{\sin(\theta+\alpha)\sin(\theta-\alpha)}{\sin\theta\cos\alpha\sin(2\theta)}, \quad (2)$$

and

$$f_{1,2}^{E1} = -i(\hat{\varepsilon}' \times \hat{\varepsilon}) \cdot \hat{z}_{1,2} F^{(1)}. \quad (3)$$

A contains the absorption correction and the Lorentz factor. In addition, α is the angle between the specular $[0,1,0]$ direction and the wave-vector transfer, and θ is half of the value of the 2θ scattering angle. The last term (Eq. 3) shows the dependence with the incident and scattered polarization vectors ($\hat{\varepsilon}$ and $\hat{\varepsilon}'$), the magnetic moment direction ($\hat{z}_{1,2}$) for each Eu ions in inequivalent sites, and the dipole matrix transition term ($F^{(1)}$).[26]

Figure 4 displays the simulated data for the two IR's (bars) and the experimental integrated intensities (symbols) obtained at the Eu L_2 edge. As shown in Fig. 4, the Eu magnetic moments follow the magnetic representation Γ_2. However, using this integrated intensity method we were not able to determine the spin direction, only distinguish between the two IR's. Therefore, FPA was performed at low temperature and at the Eu-L_2 to provide further information regarding the magnetic moment directions.

The Poincaré-Stokes parameters P_1' and P_2' as a function of the incident angle of linear polarization for the $(\frac{1}{2}, \frac{23}{2}, \tau)$ magnetic reflection are shown in Figure 5. In order to determine the Eu moment direction, the Stokes parameters displayed in Fig. 5(a) and 5(b) were fitted using the density matrix formalism[20,29–31] in which only the electric dipole transition are taken into account. The best fitting for the $P_{1,2}'$ parameters is obtained for the Eu magnetic moments following the (1,-1/2,-1) direction yielding a χ^2 value[32] of 1.25. Attempts with different spin moment directions were performed, as for instance the moments parallel to the b- and a-axis in which is built the solid lines in Fig.5(c) and 5(d), respectively. The χ^2 values for the magnetic moments along the a-, b- and c-directions are of 7.04, 29.68 and 42.14, respectively.

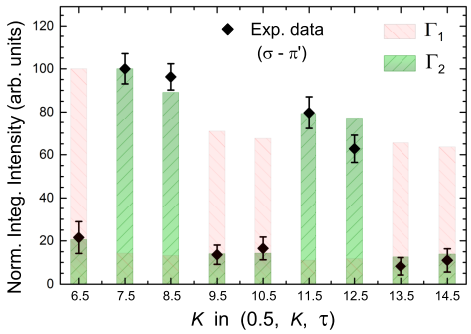

FIG. 4. (Color online) Calculated and experimental integrated intensities for the magnetic reflections $(\frac{1}{2}, \frac{K}{2}, \tau)$ with $K = (2n+1)$ performed at the Eu-L_2 absorption edge in the σ-π' channel. The calculated intensities are obtained for the two magnetic representations Γ_1 and Γ_2. The experimental error bars are extracted from the fitting function.

B. Measurements under magnetic field

In order to elucidate a possible spin-flop transition reported in macroscopic measurements[12,15], XRMS measurements were conducted under magnetic. Figure 6 reports the magnetic field dependence of the superlattice reflection $(-\frac{1}{2}, \frac{31}{2}, \tau)$ at 2.5 K for both $\pi-\pi'$ and $\pi-\sigma'$ polarization channels. A magnified view around the phase transition is being shown in the inset of Fig. 6 panel (a). In addition, Fig. 6(b) and 6(c) report the derivative of the integrated intensity and the τ dependency, respectively, as a function of magnetic field through the phase transition. Around 3 T it is observed a smooth decrease in the intensity for the $\pi - \pi'$ channel (black squares) whereas in the $\pi - \sigma'$ channel (red circles) occurs the opposite. From Fig. 6 (b) it is possible to affirm that the $EuPtIn_4$ material presents a magnetic phase transition above 3.5 T.

The evolution of the τ vector extracted from the measurements in the $\pi - \sigma'$ channel as a function of field

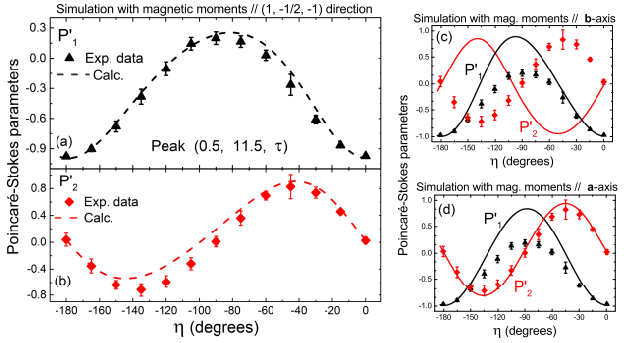

FIG. 5. (Color online) Poincaré-Stokes parameters (P_1' and P_2') obtained for the $(\frac{1}{2}, \frac{23}{2}, \tau)$ reflection. Panels (a) and (b) show the experimental Stokes parameters (symbols) and the simulations (solid lines) according to the magnetic moment parallel to the (1, -1/2, -1) direction. Panels (c) and (d) exhibits P_1' and P_2' experimental data and solid lines obtained from simulations assuming the magnetic moments parallel to the b- and a-axis, respectively.

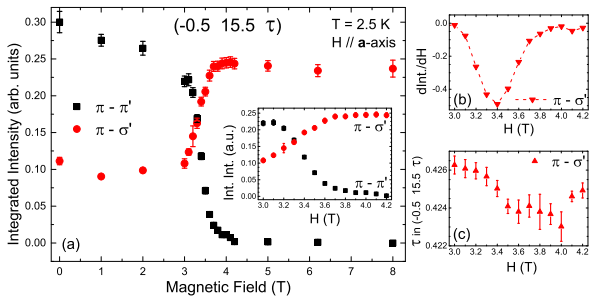

FIG. 6. (Color online) Magnetic properties observed at 2.5 K for the (-$\frac{1}{2}$, $\frac{31}{2}$, τ) peak with the magnetic field applied along the a-axis in both $\pi-\pi'$ and $\pi-\sigma'$ polarization channels. (a) Integrated intensity as a function of magnetic field. The inset shows in detail the evolution of the two polarization channels. (b) Derivative of the magnetic intensity and (c) evolution of the component τ of the propagation vector as a function of field obtained for the $\pi-\sigma'$ polarization channel.

is reported in Panel 6(c). Although the external magnetic field induces an Eu spin moment reorientation, the magnetic field has no influence in the propagation vector. Since there is a change in spin configuration under higher fields, FPA measurement was carried out at 5 T to determine the magnetic structure.

Figure 7 displays the Poincaré-Stokes parameters obtained under 5 T. The P_1' parameter exhibits a sinusoidal behavior between ±1 with a minimum around -90°, while the P_2' parameter has a completely different behavior in which it stays close to zero for the entire range. Simulations were ran to determine the spin structure and the best fitting is shown as red and black dashed lines in Fig. 7. The spin structure at 5 T is characterized by

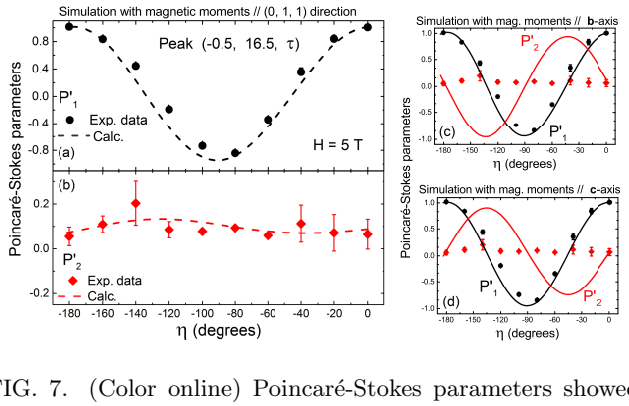

FIG. 7. (Color online) Poincaré-Stokes parameters showed as a function of the incident x-ray polarization. The black and red symbols indicate the experimental data whilst the dashed and solid lines show the fit results for a determined direction of the Eu magnetic moments. The measurements were performed in the superlattice peak (-$\frac{1}{2}$, $\frac{31}{2}$, τ) at 2.5 K and 5 T.

rotation of the magnetic moment to the bc-plane, i.e., along the $(0, 1, 1)$ direction in which the calculated χ^2 value is 0.74. The panels (b) and (c) in Fig. 7 also exhibit the simulation performed for the Eu spin moments exclusively along the b- and c-crystallographic directions. As can be seen, the P_1' component agrees quite well with the experimental data for both directions albeit the P_2' parameter is far for the agreement. The χ^2 values for the magnetic moments parallel only to the c- or b-axis are 5.11 and 6.43, respectively.

IV. DISCUSSION

The determination of the magnetic structure provides a direct view of how the magnetic ions are coupled and, therefore, a better understanding of the magnetic properties in a microscopic level. As shown in reciprocal space scan through the L component, the $EuPtIn_4$ material has an ICM phase at low temperature in which the τ component of the magnetic propagation vector is almost temperature and magnetic field independent. Although the incommensurate phase is present and the system can be visualized as triangular lattice (Figure 8, II-I-II), the ratio between the Curie constant and the temperature transition (frustration ratio, $f \equiv |\theta_{CW}|/T_N$)[35] is close to 1, which demonstrates a non-frustrated system. The FPA performed without external field indicates that the Eu magnetic moments are following the (1,-1/2,-1) direction. Attempts with the magnetic moments in different orientations were performed to confirm the spin structure. As this is first time that the magnetic structure of this family is reported and exotic properties were found, we believe it will open new perspectives to further investigate new compounds with different transition metals.

When compared to other members of this family so far studied ($EuTIn_4$), the Néel temperature is strongly affected in which $EuNiIn_4$ has the highest value ($\sim$ 16 K) while $EuIrIn_4$ has shown the magnetic ordering below 5.4 K. Figure 8 shows the evolution of the Néel temperature as a function of the b/a and b/c ratios for different $EuTIn_4$ materials. The Fig. 8 also displays the crystallographic unit cell with the rare earth and the transition metal ions (In ions were omitted to simplify the visualization). As seen there exist a trend in T_N, except for the Iridium compound, in which the magnetic temperature transitions increase when the b/a and/or b/c ratios increase. Since the only modification is the replacement of the transition metal, it suggests that the lattice parameters and therefore the electronic configuration of the transition metal ions play a relevant role in the Eu-Eu indirect exchange interactions. This effect is mainly observed when compared the samples based on Au and Ni ions. $EuAuIn_4$ has the Eu-Eu distance in the nearest neighbors (Fig. 8, distance I) located approximately 4.608 Å which is about 3% larger than the $EuNiIn_4$ (4.473Å). Although this is a small enlargement of the a-axis, it is enough to drastically reduce T_N by a

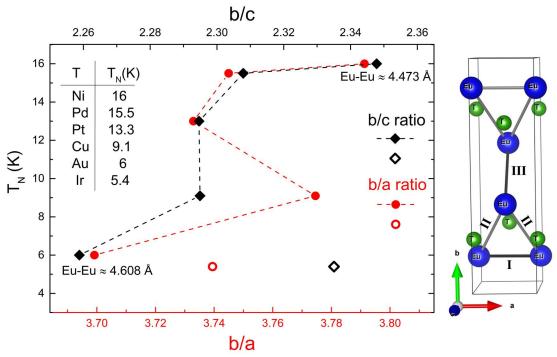

FIG. 8. (Color online) Evolution of the Néel temperature as a function of the b/a and b/c ratios observed for the EuTIn$_4$ materials. The inset exhibits the magnetic ordering temperature for each material with the respective transition metal. The crystallographic unit cell with only the Eu and the T ions is also displayed. The In ions were removed from the unit cell to a proper visualization.

factor 2-3. Therefore both magnetic ordering temperature and spin structure will be influenced. In addition, the distance between the Eu-Eu placed along the b-axis are longer in which the distances labeled with II and III are approximately 6.054 and 5.681 Å, respectively, for the EuAuIn$_4$ material. It demonstrate that this family could be naively visualized as a 1-D magnetic chain. This observation agrees with the electron spin resonance (ESR) measurements in which there are different magnetic interactions in and out of the ac-plane.[12] However, further investigation might be conducted in this family to elucidate these properties.

A pertinent example is also observed in the magnetic transition induced by external magnetic field. Several members of this family display spin-reorientation induced by magnetic field around 2-4 T which becomes these materials a playground for interesting physical phenomena. In addition, since the other members of this family have displayed similar behavior, particularly in isothermal magnetization measurements, we believe that these materials are good candidates to host also incommensurate spin structures.

In addition to the magnetic structure determination, we focus our attention to explain the different anomalies observed in macroscopic measurements to corroborate them with our findings. Two independent heat capacity measurements observed besides the AFM ordering at $\sim$ 13.3 K, a broad feature around 5.5 K[9,12]. The broad feature is also observed in the EuNiIn$_4$ compound and it is not related to a change in the magnetic structure but it might be related to degeneracy of $4f$ states. This anomaly at low temperature is frequently seen in compounds based on $4f^7$ elements, i.e. Eu^{2+} and Gd^{3+}.[13,33] In addition, Rosa *et al.* [12] reported a small sharp anomaly in the specific heat at 12.6 K (T^*) in which it could be related to a second magnetic phase transition. As can be seen in our temperature dependence, we could not find any evidence of a second phase transition taking place below T_N, i.e. around macroscopic anomaly T^*. A magnetic anomaly related to the Eu ions such as a spin reorientation induced by thermal energy would be noted in the XRMS temperature dependence measurements. Distinct magnetic reflections (not displayed here) with smaller K component in which could be possible observed rearrangement of the magnetic structure in the ac-plane yielded similar temperature evolution, i.e., without any anomaly feature at 12.6 K. The τ component and the peak width reported in Fig. 3 have not also displayed any anomaly feature around T^* which would support an additional magnetic transition. Therefore, one can rule out that there may exist a second magnetic phase transition induced by temperature at T^*.

Regarding the spin-flop transition, Hedo *et al.* [15] exhibited two critical field along different crystallographic directions. When the magnetic field is parallel to $[0,0,1]$ direction, the transition takes place around 2.5 T while the field pointing along the $[1,0,0]$ yields a critical value around 3.5 T. This later spin-flop transition was observed in our XRMS measurements at similar field value and it is related to a rotation of the Eu spin moments away from the a-axis. As reported in the FPA measurements under 5 T parallel to $[1,0,0]$ direction, the magnetic field is able to move away the moments mainly from the a-axis. Therefore the magnetic structure above the critical field has shown the spin in the bc-plane. Although the magnetic field is sufficient to manipulate the magnetic structure, the incommensurate propagation vector component τ is barely affected since there is a variation of $\Delta\tau \sim 0.003$. This could be explained due to the fact that the ICM phase is attached to the geometry of the Eu ions positions inside the unit cell. It will be also interesting to see how the propagation vector changes when the transition metals are changed in this system. Therefore we believe there are a lot of works to be conducted in this system.

V. SUMMARY

We have determined the EuPtIn$_4$ magnetic structures at low temperature and under an external magnetic field using the XRMS technique. The x-ray scattering measurements exhibited an interesting incommensurate antiferromagnetic structure with a magnetic propagation vector $(\frac{1}{2},\frac{1}{2},\tau)$ with $\tau \sim 0.428$ in which we assumed that only the Eu ions carried non null magnetic moment. The incommensurability presents along the c-axis was observed to be almost temperature and magnetic field variant. Full polarization analysis performed below $T_N \sim$ shows that the Eu^{2+} moment aligned along the (1,-1/2,-1) direction and it rotates to the $(0,1,1)$-direction when a magnetic field higher than 3.5 T is applied along the a-axis. No further transitions induced by temperature or due to Eu^{3+} contribution are found as a function of temperature. The evolution of the magnetic integrated in-

tensity for the superlattice peak $(-\frac{1}{2}, \frac{31}{2}, \tau)$ as a function of magnetic field indicates that the Eu moment direction is strongly affected, whereas the propagation vector barely changes above the magnetic transition around $\sim$ 3.5 T. These findings corroborate quite well the macroscopic measurements performed under magnetic field.

ACKNOWLEDGMENTS

This work was carried out at the light source PETRA III at DESY, a member of the Helmholtz Association (HGF). We are indebted to D. Reuther and R. Kirchhof for their assistance at P09/DESY.

[1] J.D. Thompson and Z. Fisk, J. Phys. Soc. Jpn **81**, 011002 (2012).

[2] R. Movshovich, M. Jaime, J. D. Thompson, C. Petrovic, Z. Fisk, P. G. Pagliuso, and J. L. Sarrao, Phys. Rev. Lett. **86**, 5152 (2001).

[3] J. Thompson, R. Movshovich, Z. Fisk, F. Bouquet, N. Curro, R. Fisher, P. Hammel, H. Hegger, M. Hundley, and M. Jaime, J. Magn. Magn. Mater. **226**, 5 (2001).

[4] Wei Bao, P. G. Pagliuso, J. L. Sarrao, J. D. Thompson, Z. Fisk, and J. W. Lynn, Phys. Rev. B **64**, 020401(R) (2001).

[5] P. G. Pagliuso, J. D. Thompson, M. F. Hundley, J. L. Sarrao, and Z. Fisk, Phys. Rev. B **63**, 054426 (2001).

[6] R. M. Rykhal', O. S. Zarechnyuk, Ya. P. Yarmolyuk, Sov. Phys. Crystallogr., **17**, 453 (1972).

[7] R. Pöttgen, R. Mullmann, B. D. Mosel, and Hellmut Eckert, J. Mater. Chem. **6**, 801 (1996).

[8] R.-D. Hoffmann and R. Pöttgen, Chem. Eur. J. **6**, 4 (2000).

[9] P. Kushwaha, A. Thamizhavel, A. K. Nigam, S. Ramakrishnan, Cryst. Growth Des. **14**, 2747 (2014).

[10] S. Sarkar, M. J. Gutmann, and S. C. Peter, Dalton Trans. **43**, 15879 (2014).

[11] H. Shishido, N. Nakamura, T. Ueda, R. Asai, A. Galatanu, E.Yamamoto, Y. Haga, T. Takeuchi, Y. Narumi, T. C. Kobayashi, K. Kindo, K. Sugiyama, T. Namiki, Y. Aoki, H. Sato, and Y. Onuki, J. Phys. Soc. Jpn., **73**, 664 (2004).

[12] P.F.S. Rosa, C.B.R. de Jesus, Z. Fisk, P.G. Pagliuso, J. Magn. Magn. Mater. **371**, 5 (2014).

[13] W. Schnelle, R. K. Kremer, R.-D. Hoffmann, U. Ch. Rodewald, and Rainer Pöttgen, Z. Naturforsch. 69b, 1003 (2014).

[14] S. Ikeda, Y. Tanaka, and H. Kobayashi, JPS Conf. Proc. **3**, 014023 (2014).

[15] M. Hedo, Y. Hiranaka, A. Nakamura, K. Tomori, F. Honda, Y. Haga, H. Harima, K. Matsubayashi, Y. Uwatoko, T. Nakama1, and Y. Onuki, J. Phys.: Conden. Series **592**, 012047 (2015).

[16] J. Strempfer, S. Francoual, D. Reuther, D. K. Shukla, A. Skaugen, H. Schulte-Schrepping, T. Kracht and H. Franz, J. Synchrotron Rad. **20**, 541 (2013).

[17] B. Detlefs, S. B. Wilkins, R. Caciuffo, J. A. Paixão, K. Kaneko, F. Honda, N. Metoki, N. Bernhoeft, J. Rebizant, and G. H. Lander, Phys. Rev. B **77** 024425 (2008).

[18] R. D. Johnson, S. R. Bland, C. Mazzoli, T. A. W. Beale, C. H. Du, C. Detlefs, S. B. Wilkins, and P. D. Hatton, Phys. Rev. B **78** 104407 (2008).

[19] S. Francoual, J. Strempfer, D. Reuther, D. K. Shukla, and A Skaugen, J. Phys.: Conden. Matter **425**, 132010 (2013).

[20] C. Mazzoli, S. B. Wilkins, S. DiMatteo, B. Detlefs, C. Detlefs, V. Scagnoli, L. Paolasini, and P. Ghigna, Phys. Rev. B **76** 195118 (2007).

[21] A.C. Thompson, et al. X-Ray Data Booklet, Center for X-ray Optics and Advanced Light Source 2nd edn Lawrence Berkeley Laboratory, University of California (2009).

[22] A. Stunault, K. Dumesnil, C. Dufour, C. Vettier, and N. Bernhoef, Phys. Rev. B **65** 064436 (2008).

[23] S. Blundell, *Magnetism in Condensed Matter* (Oxford Master Series in Condensed Matter Physics, 2001).

[24] M.F. Collins, *Magnetic Critical Scattering* (Oxford University Press, Oxford, 1989)

[25] A. Wills, Physica B **276**, 680 (2000).

[26] J. P. Hannon, G. T. Trammell, M. Blume, and D. Gibbs. Phys. Rev. Lett., **61**, 1245-1248, (1988).

[27] J. Hill and D. McMorrow, Acta Cryst. A **52**, 236 (1996).

[28] C. Detlefs, A. H. M. Z. Islam, A. I. Goldman, C. Stassis, P. C. Canfield, J. P. Hill, and D. Gibbs, Phys. Rev. B **55**, 680 (1997).

[29] V. Scagnoli, C. Mazzoli, C. Detlefs, P. Bernard, A. Fondacaro, L. Paolasini, F. Fabrizi, and F. de Bergevin, J. Synchrotron Radiat. **16**, 778 (2009).

[30] C. Detlefs, M. Sanchez del Rio, and C. Mazzoli, Eur. Phys. J. Spec. Top. **208**, 359–371 (2012).

[31] S. Francoual, J. Strempfer, J. Warren, Y. Liu, A. Skaugen, S. Poli, J. Blume, F. Wolff-Fabris, P. C. Canfield, and T. Lograsso, J Synchrotron Radiat. **22**, 1207-1214 (2015).

[32] The χ^2 value is estimated through: $\chi^2 = \sum_i (O_i - S_i)^2/|S_i|$, where O_i are the observed experimental data and S_i are the simulations data.

[33] S. Seiro and C. Geibel, J. Phys.: Conden. Matter **23**, 375601 (2011).

[34] H. Stragier, J. O. Cross, J. J. Rehr, Larry B. Sorensen, C. E. Bouldin, and J. C. Woicik, Phys. Rev. Lett. **69**, 3064 (1992).

[35] A. P. Ramirez, Annu. Rev. Mater. Sci. 24, 453 (1994).